

This is an Open Access document downloaded from ORCA, Cardiff University's institutional repository: <https://orca.cardiff.ac.uk/id/eprint/94391/>

This is the author's version of a work that was submitted to / accepted for publication.

Citation for final published version:

Marega, Riccardo, Prasetyanto, Eko Adi, Michiels, Carine, De Cola, Luisa and Bonifazi, Davide 2016. Fast targeting and cancer cell uptake of luminescent antibody-nanozeolite bioconjugates. *Small* 12 (39) , pp. 5431-5441. 10.1002/sml.201601447

Publishers page: <http://dx.doi.org/10.1002/sml.201601447>

Please note:

Changes made as a result of publishing processes such as copy-editing, formatting and page numbers may not be reflected in this version. For the definitive version of this publication, please refer to the published source. You are advised to consult the publisher's version if you wish to cite this paper.

This version is being made available in accordance with publisher policies. See <http://orca.cf.ac.uk/policies.html> for usage policies. Copyright and moral rights for publications made available in ORCA are retained by the copyright holders.



DOI: 10.1002/sml.201500879

Article type: Full Paper

Fast targeting and cancer cell uptake of luminescent antibody-nanozeolite bioconjugates

Riccardo Marega, Eko Adi Prasetyanto, Carine Michiels, Luisa De Cola and Davide Bonifazi**

Dr. R. Marega, Prof. Dr. D. Bonifazi
Namur Research College (NARC) and Department of Chemistry, University of Namur, Rue de Bruxelles 61, Namur, B-5000, Belgium
E-mail: davide.bonifazi@unamur.be

Dr. E. A. Prasetyanto, Prof. Dr. L. De Cola
Institut de science et d'Ingénierie Supramoléculaire (ISIS), Université de Strasbourg, 8 Rue Gaspard Monge, BP 70028, F-67000 Strasbourg, France and Karlsruher Institut für Technologie KIT-INT, Karlsruhe, D-76131, Germany
E-mail: decola@unistra.fr

Prof. Dr. C. Michiels
Cellular Biology Research Unit - NARILIS, University of Namur, Rue de Bruxelles 61, Namur, B-5000, Belgium

New Address: Prof. Dr. D. Bonifazi
School of Chemistry; Cardiff University, Park Place, CF10 3AT, Cardiff, United Kingdom.
E-mail: BonifaziD@cardiff.ac.uk

Keywords: nanomaterials, targeting, cellular uptake, zeolites, Cetuximab

Abstract

Understanding the targeted cellular uptake of nanomaterials is an essential step to engineer and program functional and effective biomedical devices. In this respect, here we describe the targeting and ultra-fast uptake of zeolite nanocrystals functionalized with Cetuximab antibodies (Ctxb) by cells overexpressing the epidermal growth factor receptor. Biochemical assays showed that the cellular uptake of the bioconjugate over the targeted cancer cells already begun 15 minutes after incubation, at a rate around 10-fold faster than that observed in the negative control cells. These findings further show the role of Ctxb exposed at the surfaces of the zeolite nanocrystals in mediating the targeted and rapid cellular uptake. By using temperature and pharmacological inhibitors as modulators of the

internalization pathways, our results univocally suggest a dissipative uptake mechanism of these nanomaterials, which seems to occur using different internalization pathways, according to the targeting properties of these nanocrystals. Owing to the ultra-fast uptake process, harmless for the cell viability, these results further pave the way for the design of novel theranostic tools based on nanozeolites.

1. Introduction

Strong hope is nowadays devoted on nanostructured materials as functional carriers for therapy and diagnostic applications.^[1] Many of the proposed nanotechnological approaches can in principle bring crucial solutions in medicine, and preliminary demonstrations in preclinical or clinical trials were reported from several laboratories throughout the world.^[2] Among the different applications, nanomaterials are under thorough investigation for cancer theranostics^[3] due to their wide chemical versatility to impart multifunctionality^[4] and their possibility to accumulate at the tumor district by enhanced permeation and retention effect^[5] (EPR). However, an important drawback limiting their clinical exploitation entails the inadequate *in-vivo* accumulation at the targeted site and the consequent intracellular localization due to physiological clearance mechanisms such as the mononuclear phagocyte system (MPS) uptake.^[6] It is therefore of paramount importance to reduce the nanomaterial extracellular concentrations. Depending on their structural and morphological properties (i.e. chemical composition, shape, size and charges), several classes of nanomaterials have been found to cross cell membranes through different and sometimes controversial internalization mechanisms, such as endocytosis or membrane penetration.^[7] Understanding the internalization mechanism of a given nanomaterial is thus an essential step to engineer and program functional nanomaterials for hierarchical targeting and drug-delivery applications.^[8]

Current design of nanomaterial for cancer theranostics rely on the use of anchored ligands^[2d,9] (i.e. folic acid^[10] or hyaluronic acid^[11]) to impart targeting properties and receptor mediated endocytosis (RME).^[12] Antibody bioconjugation is an even more convenient strategy for nanomaterial

functionalization because, compared to other ligand-based approaches, yielded derivatives retaining their biological properties even in serum supplemented medium, being thus resistant to the biological modulation by the protein-corona.^[13] Monoclonal antibody Cetuximab^[14] (Ctxb) is one of the best candidates to target the epidermal growth factor receptor (EGFR), a marker overexpressed in several kind of cancers.^[15] In this respect, Ctxb nano-bioconjugates retained such epitope targeting,^[15c,16] thus displaying fast *in-vitro* internalization (already 30 minutes after incubation),^[16e,16j,16k] enhanced uptake compared to pegylated materials (about 15-fold 2 hours after incubation), and resilient *in-vivo* accumulation at the tumor site.^[15c,16a,16c,16h,17]

Due to their peculiar physicochemical properties and payload delivery capacity, silica-based nanomaterials are largely explored nowadays for biomedical applications,^[4b,18] with some examples of nanoparticle-antibody hybrids showing enhanced binding to cancer cells and tumor accumulation.^[15c,19] In this respect, zeolite nanocrystals emerged as potent biomedical tools for imaging applications and as a platform for cell growth and interactions,^[20] since they show defined shape and size distributions, and are made of an inorganic framework that allows for both encapsulation of luminescent probes and exohedral surface modification. In particular, organic functionalized zeolites were efficiently internalized by HeLa cells within 2 and 24 hours, with differences in the intracellular accumulation depending on the surface functionalities (carboxyl, amino, poly-ethyleneglycol or poly-allylamine moieties).^[21] In a consecutive study, the group of De Cola further described that zeolite nanocrystals, coated with a biodegradable poly-L-lysine, could be internalized already one hour after incubation suggesting a fast intracellular payload delivery.^[20f] Nonetheless, this material lacks of specific binding moieties or targeted cellular accumulation properties.

In this work, we report on the targeting action and fast cancer cell uptake of fluorescent zeolite nanocrystals functionalized with Ctxb antibodies. We observed selective binding of the nano-bioconjugate to EGFR+ cells, model of epidermoid carcinoma cells, followed by a rapid uptake occurring already 15 minutes after addition of the nanomaterial. Temperature- and

pharmacologically-modulated internalization studies suggest a dissipative accumulation mechanism involving different internalization pathways.

2. Results and discussion

By exploiting previously established protocols,^[21,22] L-zeolite nanocrystals were prepared, endohedrally equipped with the red-emitter oxazine-1 fluorophore, and exohedrally functionalized with amino-PEG silane (molecular weight about 5,000 gmoL⁻¹), yielding luminescent Zeo-NH₂. As revealed by porosimetry, TEM and DLS measurements (see section S1), these protocol generates porous nanocrystals of around 50-60 nm retaining the red emissive properties of the cavity-confined fluorophore (Figures S1d-e). As expected, upon pegylation, the hydrodynamic diameter of the resulting Zeo-NH₂ nanoparticles increases to ca. 86 nm (Table 1 entries 1 and 2, and Figures S1f-g). Ctxb antibody was covalently linked to the nanomaterial by adapting a previously developed carbodiimide-mediated amidation protocol^[16a,23] to yield the targeting nanozeolite derivative, Zeo-NHCO-Ctxb (**Scheme 1**, path a). Since it is known that proteins can irreversibly adsorb onto a large variety of nanostructured materials,^[24] we verified the occurrence of aspecific Ctxb immobilization onto Zeo-NH₂ also in the absence of the coupling agent (Zeo-NH₂/Ctxb, Scheme 1 path b). X-ray photoelectron spectroscopy (XPS, see section S2) of Zeo-NH₂ material showed the expected elemental composition (O, Si, C, Al, N) fingerprinting the presence of the ethylene glycol C atoms (292-298 eV, **Figure 1a**) and of the terminal amino groups (less than 1 at% of N atoms, Figure 1b). XPS spectra of both Zeo-NHCO-Ctxb and Zeo-NH₂/Ctxb clearly display the contemporaneous presence of C-centered peaks fingerprinting both the ethylene glycol and the polypeptidic molecular fragments (Figure 1a) along with an enhanced content of N atoms (around 11 at%), both supporting the occurrence of the bioconjugation. By defining the “organic-to-inorganic proportion” as the ratio between the sum of C1s and N1s at% divided by the sum of Si2p and Al2p at%, we obtained values of 0.4 for Zeo-NH₂ and of about 4.0 for Zeo-NHCO-Ctxb and Zeo-NH₂/Ctxb, revealing a comparable loading of Ctxb for the covalent vs non-covalent anchoring of the antibody. Similar findings also

resulted from a “bulk” characterization such as thermogravimetric analysis (TGA), performed both under N₂ (to assess pyrolysis, Figure 1c) and air atmosphere (Figure S3). As expected, the TGA traces for the sample containing Zeo-NH₂ confirmed the low amount of the organic content and oligoethylene-derived pyrolysis,^[25] whereas the characteristic weight loss profile (minimum at around 320 °C, Figure 1c) underpinning the presence of Ctxb is clearly visible for both Zeo-NHCO-Ctxb and Zeo-NH₂/Ctxb.^[16a,23] The Ctxb loading resulted to be 2.0 and 1.7 nmolmg⁻¹ for hybrids Zeo-NHCO-Ctxb and Zeo-NH₂/Ctxb, respectively (see S3).

To further unravel the necessity and efficacy of the covalent bioconjugation protocol, we analyzed the zeolite derivatives through fluorescence revelation after gel electrophoresis separation. Indeed, the cavity-confinement of the oxazine-1 fluorophore allows for the intrinsic detection of the zeolite framework ($\lambda_{\text{exc}} = 633$ nm), whereas the amino groups of both PEG-NH₂ moiety and antibody can be easily labelled with a specific green fluorescent dye (Cy2® NHS, $\lambda_{\text{exc}} = 488$ nm). This consents the discrimination between the covalent- and loosely-bound Ctxb moieties (see Figure 1 and S4). As references, lanes 1, 2 and 3 were loaded with three different amounts of Ctxb (approximately 66, 44 and 22 fmol, respectively), whereas the lanes 4, 5 and 6 were loaded with the zeolite materials (Zeo-NH₂, Zeo-NHCO-Ctxb and Zeo-NH₂/Ctxb from 1.0 mgmL⁻¹ solutions, approximately 0, 40 and 34 fmol of Ctxb, respectively). After gel electrophoresis, the Ctxb bands located at about two-thirds of the migration path, and show dose-dependent fluorescence intensities in the reference lanes 1,2 and 3. On the contrary, lane 4, tracing Zeo-NH₂, displayed no green fluorescence due to the absence of Ctxb and the low amount of PEG-NH₂ moiety. Lanes 5 and 6, respectively tracing Zeo-NHCO-Ctxb and Zeo-NH₂/Ctxb derivatives, showed co-localized green and red fluorescence at the deposition spots and a great release of free Ctxb for the hybrid prepared in the absence of the coupling agent (Zeo-NH₂/Ctxb). This supports the idea for which non-negligible supramolecular interactions might occur between Ctxb and the nanomaterial, favoring a non-covalent association, as previously observed with CNT materials.^[23a,26] Nonetheless, the use of the carbodiimide-mediated ligation protocol irreversibly strengthened the association between the two counterparts, as previously

reported for AuNPs-Ctxb and CNT-Ctxb analogues.^[16a,23] It is known that serum proteins can adsorb onto the nanoparticle surface,^[24,27] with some literature examples reporting dramatic diameter increases after protein corona formation (*i.e.*, 2- to 10-fold for citrate-capped AuNPs of 15, 40 and 80 nm).^[28] Given these premises, we determined the hydrodynamic diameters of Zeo-NH₂ and Zeo-NHCO-Ctxb, in serum supplemented medium (DMEM + 10% fetal bovine serum), which resulted to be 110 nm (PDI 0.113, **Table 1** entry 2) and 117 nm (PDI 0.300, Table 1 entry 3), respectively. By further monitoring the dispersions as a function of the incubation time (0.5, 7, and 24h), one can clearly notice a minor increase of the size distributions up to 24h (109.5 ± 28.7 nm, 108.6 ± 28.6 nm, and 113.7 ± 28.3 nm for Zeo-NH₂, and 136.6 ± 67.2 nm, 143 ± 67.4 nm, and 152.1 ± 66.6 nm for Zeo-NHCO-Ctxb, after 0.5h, 7h and 24h), thus suggesting reduced protein adsorption and limited particle aggregation, in line with what found for other PEGylated nanomaterials.^[29] Notably, no signature of free Ctxb was observed in the samples containing Zeo-NHCO-Ctxb (see S5), which suggests the lack of a Ctxb “soft corona” in line with the gel-electrophoresis findings. Regarding the particle electrophoresis, Ctxb, Zeo-NH₂, and Zeo-NHCO-Ctxb displayed negative ζ potential values of around -8.9 mV, -22.7 mV, and -35.7 mV, respectively, proving the progressive increase of positive charges due to the presence of amino-PEG and Ctxb moieties (Table 1 entries 2,3 and 4).

Aiming at assessing a possible effect of the zeolite nanocrystals on the cell viability, we have incubated both EGFR+ cells and EGFR- cells with Zeo-NHCO-Ctxb and Zeo-NH₂ at equivalent nanocrystal concentrations (0 – 0.16 mgmL⁻¹, **Figure 2**). It is known that nanoparticles can interfere with the common reagents used for assessing cell viability due to the spectral overlap or fluorescence quenching, amongst others.^[30] Since our luminescent nanocrystals may interfere with the reagents of cytotoxicity assays based on either red-absorbing chromophores (*i.e.*, resazurin or trypan blue), or fluorescent probes (*i.e.*, Rhodamine derivatives or Ethidium bromide/acridine orange), we have adapted the MTS assay protocols (see section S6) to assess the cell viability. As displayed in the cell viability plot (Figure 2), one can exclude a dramatic effect of all nanomaterials on the cell viability of both EGFR+ and EGFR- cell lines after 24h of incubation.

To verify whether Zeo-NHCO-Ctxb retained the key property like other Ctxb-exposing nanomaterials of binding preferentially EGFR⁺ cells over those EGFR⁻, we selected human epidermoid carcinoma A431 cells, overexpressing the epitope EGFR (EGFR⁺), and human endothelial cells (EAhy926 cells), which do not express this receptor (about 200-fold less, see Table S7).^[16a,23] The selection of the EAhy926 cells as the negative control is dictated by the necessity of evaluating the aspecific binding and internalization by the components of the endothelial barrier, which can lead to an *in-vivo* extravasation of the nanomaterial, further reducing the bioavailability at the tumor site.^[16a,23] Confocal microscopy analysis of EGFR⁺ cells incubated with Zeo-NHCO-Ctxb allowed for the cell identification through the far-red channel, clearly displaying a positive response between the targeted cells and the fluorescent nanomaterial (see Section S8). By repeating the test with the negative control, no cell identification was possible through the far-red channel, which showed Zeo-NHCO-Ctxb particles randomly fluctuating in the medium and thus lacking any kind of targeting action toward EGFR⁻ cells (see Section S9). This observation is supported by the results from cell-based ELISA experiments onto adherent cells, which reported higher binding events of Zeo-NHCO-Ctxb onto the EGFR⁺ cells compared to the negative controls (Figure S10).^[16a,23a] We next assessed whether Zeo-NHCO-Ctxb could detect the presence of EGFR⁺ cells in a mixed suspension with the negative control. To this aim, we labelled EGFR⁻ cells with a green fluorescent dye (Vybrant® DIO, $\lambda_{\text{exc}} = 488 \text{ nm}$), mixed with unlabeled EGFR⁺ cells (about 1:1 ratio), and added Zeo-NHCO-Ctxb. The resulting mixture was incubated for 2.5 min, and then analyzed through confocal microscopy (**Figure 3**). The suspended EGFR⁺ and EGFR⁻ cells possess similar shape and size, and cannot be discriminated by the differential interference contrast (DIC) channel (Figure 3, row a). Excitation at 488 nm clearly revealed the labelled EGFR⁻ cells (Figure 3, row b), while excitation at 633 highlighted the EGFR⁺ ones (Figure 3, row c). The overlay of the three channels unambiguously allowed the color-based identification of the cells types in the suspension, being the EGFR⁺ cells stained in red due to the targeting and luminescent zeolites, and the EGFR⁻ cells colored only in green due to the pre-staining procedure (Figure 3, row d). These binding studies highlight that, regardless

of the use of adherent or suspended cells (for ELISA and confocal microscopy, respectively) or the incubation media (serum-free for ELISA, serum-containing medium for confocal microscopy), Zeo-NHCO-Ctxb always binds rapidly and specifically to the EGFR⁺ cells.

In order to unravel the internalization process and to study the uptake mechanisms (*i.e.*, through physical membrane permeation or endocytosis),^[7] we prepared adherent cells and performed both flow cytometry and confocal microscopy investigations.^[31] Regarding the flow cytometry analysis, since the nanomaterial uptake depend on several factors, we have determined the extent of the uptake by fixing two levels for 3 variables, such as the “cell type” (EGFR⁺ cells or EGFR⁻ cells), the “cell medium” (10% serum or serum-free medium), the “nanomaterial” (Zeo-NHCO-Ctxb or Zeo-NH₂ nanoparticles) and 6 levels for the variable “incubation time” (15, 45, 95, 150, 360 or 1440 min). The resulting 48 experimental combinations were performed in independent sets of experiments, to gather a dataset amenable for both graphical representation of the time-dependent uptake profiles (Figure S11), as well as statistical evaluation. The degree of the uptake is reported as absolute values (% of positive cells, **Figures 4a-c**) and normalized values ($[(\% \text{ of positive cells}) / \text{highest } \% \text{ of positive cells}] \times 100$), the latter better highlighting the internalization speed (Figures 4b-e). The uptake profiles qualitatively indicate that, after short incubation times (range 15 – 150 min), Zeo-NHCO-Ctxb always determine enhanced staining compared to Zeo-NH₂, with the latter requiring prolonged incubation time to reach the maximal uptake (360 or 1440 min). By defining IT₅₀ as the incubation time necessary to reach half of the highest staining proportion, it is possible to estimate the IT₅₀ values for Zeo-NHCO-Ctxb that reveal to be 15 – 45 and 95 – 150 min for the EGFR⁺ cells and EGFR⁻ cells, respectively. On the contrary, non-targeting Zeo-NH₂ displayed IT₅₀ values of 150 – 360 and 360 – 1440 min for the EGFR⁺ cells and EGFR⁻ cells, respectively. The statistical evaluation of the normalized values by one-way analysis of variance (ANOVA) unambiguously suggests a fast internalization of the Ctxb-bioconjugated particles by the EGFR⁺ cells (Figures 4c-f).

Two-way ANOVA assessments can elucidate different aspects of the uptake regulation, such as the influence of factors accounting for one specific variable (*i.e.*, “incubation time”), or two variables

(*i.e.*, “nanomaterial biological interface”, which combines “nanomaterial” and “cell medium”) and whether these factors are linked or not. We thus performed different two-way ANOVA studies. In particular, building the two-way ANOVA with the “incubation time” factor (**Figures 5a-b**) reveals a shallower uptake profile for the EGFR+ cells compared to the EGFR- cells. This further confirms that already after short incubation times the nanoparticles uptake is close to its maximal value. On the other hands, the time-independent profiles show a higher Zeo-NHCO-Ctxb uptake than that of Zeo-NH₂ (about 2 fold, Figures 5c-d) and a strong link between “incubation time” and “nanocrystal biological interface” (interaction with $p < 0.00001$ for the EGFR+ cells). Statistically significant differences and connections between the factors also emerge by using the variables “cell type” (Figure 5e, $p < 0.0001$) and “nanomaterial” (Figure 5f, $p < 0.00001$). This clearly indicates that the EGFR+ cells internalize more rapidly the zeolite nanocrystals than the EGFR- cells ($57 \pm 4\%$ vs $44 \pm 5\%$), and that the Zeo-NHCO-Ctxb particles are faster internalized than its precursor Zeo-NH₂ ($66 \pm 4\%$ vs $34 \pm 4\%$).

Taken together, all the ANOVA results indicate a faster uptake of the Ctxb nano bioconjugate by the EGFR+ cells, and that: i) incubation time; ii) cell type; iii) the presence of Ctxb are the key factors triggering the uptake of the zeolite nanocrystals. Both graphical profile and statistical analysis did not reveal any dramatic effect of the variable “cell medium” in determining statistically significant changes in the uptake, thus suggesting a limited role of the serum in affecting the cell uptake of these zeolite-based nanomaterials.

To discriminate between the effective extracellular, membrane-bound or intracellular nanocrystals localization, we fluorescently stained the nucleus by Hoechst reagent ($\lambda_{exc} = 400$ nm), cytoskeleton components (F-actin) using AlexaFluor488-Phalloidin® ($\lambda_{exc} = 488$ nm) and used cell segmentation by confocal microscopy (Figure S12a). We incubated both EGFR+ and EGFR- cells with either Zeo-NHCO-Ctxb or Zeo-NH₂ in serum containing medium for 15 or 150 minutes, since these incubation conditions were the lower limit to observe nanocrystal uptake and discriminate between the two cell lines. Experiments performed at 37 °C (**Figure 6** and S12) showed some Zeo-NHCO-Ctxb particles

surrounded by membrane invaginations or completely internalized already 15 minutes after incubation (Figure 6a). On the contrary, internalization of Zeo-NH₂ zeolites was not detected after such short incubation times (Figure 6e). After 150 minutes of incubation, several Zeo-NHCO-Ctxb particles were observed intracellularly (Figure 6b), while only few clusters of Zeo-NH₂ co-localized with membrane invaginations were detected (Figure 6f). The presence of Zeo-NHCO-Ctxb or Zeo-NH₂ nanocrystals inside the targeted cells is supported also by TEM imaging (see **Figure 7** and S13). Reference experiments performed at 4 °C displayed the blockage of the nanomaterial uptake, enhanced sedimentation and agglomeration of the nanoparticles. This was more obvious after prolonged incubation times (150 minutes, Figure 6c-d-g-h, and S14). The addition of Zeo-NHCO-Ctxb or Zeo-NH₂ to the EGFR- cells induced very few occurrences of membrane invagination and a reduced uptake over short incubation times, especially using Zeo-NH₂ (see S15).

To get a deeper insight on the intracellular localization of Zeo-NHCO-Ctxb after very short incubation times, we imaged the EGFR+ cells 15, 45 and 95 min after incubation by confocal microscopy (**Figure 8**). The optical sectioning of the corresponding images confirms that after 15 minutes of incubation some particles seem already undergoing internalization (Figure 8a and S16). At 45 minutes, it is already possible to discern the intracellular zeolites in endosomal-like structures, as revealed by co-localization with the actin filaments (Figure 8b and S17), eventually leading to a further diffusion toward the nucleus at t = 95 minutes (Figure 8c and S18). Again, the nanomaterial localization in cells incubated at 4 °C was essentially unchanged under the different incubation times, with the Ctxb-functionalized zeolitic nanoclusters predominantly situated at the periphery of the plasma membrane (Figure 8d-e-f and S19-21).

Accounting for the low impact of serum in affecting both the binding properties and the nanocrystal uptake, and of the similar colloidal properties of Zeo-NHCO-Ctxb and Zeo-NH₂ nanocrystals, these results indicate that the Ctxb moiety acts as a specific cell-recognition platform, thus driving the selective cellular uptake. Since the temperature-dependent outcomes of the internalization studies suggest a dissipative process for the uptake of these nanocrystals, we treated the EGFR+ cells with a

panel of pharmacological inhibitors^[7f,32] prior to the incubation with Zeo-NHCO-Ctxb or Zeo-NH₂. We selected hydroxy-dynasore (to block the GTPase activity of dynamin and thus dynamin-dependent endocytosis, conc. $\approx 60 \mu\text{M}$),^[33] chlorpromazine (to block the clathrin-dependent endocytosis, conc. $\approx 60 \mu\text{M}$),^[34] genistein (a tyrosine kinase inhibitor that blocks caveolae-dependent endocytosis, conc. $\approx 150 \mu\text{M}$),^[34-35] 5-(N-ethyl-N-isopropyl)-amiloride (a macropinocytosis inhibitor, conc. $\approx 30 \mu\text{M}$),^[36] and nocodazole (a microtubule-depolymerizing agent, conc. $\approx 40 \mu\text{M}$).^[37] Thanks to the steep uptake profiles, we have exposed the cells to the pharmacological inhibitors for relatively short times (60 min pre-incubation, 150 min with zeolite nanocrystals) to avoid the cytotoxic effects derived from the use of these inhibitors upon prolonged incubation times.^[32b,32c]

The resulting uptake profiles suggest that the internalization of Zeo-NHCO-Ctxb is affected by chlorpromazine, amiloride and genistein, whereas the Zeo-NH₂ uptake is reduced by dynasore (Figure S22). EGFR internalization is known to proceed through different endocytotic pathways (clathrin-caveolae-, and dynamin-dependent) depending on cell type and ligand stimulation,^[38] while the detailed mechanism and physiological relevance of Ctxb internalization remains elusive. For instance, literature data about the internalization of Ctxb-Au nanoconjugates suggest that the cell type, EGFR+ expression levels, and Ctxb/Au ratio play an important role in dictating the internalization mechanism that can occur following different pathways, spanning from dynamin dependent and independent routes to caveolar and pinocytotic uptake.^[16j,k] Considering this background and our experimental findings, it is likely that multiple effectors affect the uptake of Zeo-NHCO-Ctxb (clathrin- and caveolae-mediated endocytosis, macropinocytosis), which seems to follow another pathway than that of Zeo-NH₂ under these experimental conditions.

3. Conclusions

In conclusion, in this work we were able to control the degree of zeolite nanocrystals interaction with selected cells through antibody conjugation, and determine differences in the internalization times between cancer- and reference- cell lines. The bioconjugated nanomaterial rapidly binds to EGFR+

cells, allowing for their selective detection by confocal microscopy in a mixed population with a reference cell line. Interestingly, a different cellular uptake of the Ctxb-functionalized zeolite nanocrystals over the selected cell lines was observed already 15 minutes after incubation with the EGFR+ cells (almost ten-times faster compared to the use of non-targeting zeolite nanocrystals lacking of the targeting antibody). Furthermore, preliminary cytotoxicity investigations excluded significant reduction of the cell viability under the chosen experimental conditions. Along with some recent literature results,^[2d,39] these findings further suggest that the nanomaterial bioconjugation with antibodies represents a valuable strategy for the fast intracellular accumulation of nanoparticles, consequently limiting physiological clearance processes that are currently hindering the marketing potential of several nanomaterials. Considering the wide pool of antibodies approved by the FDA in the US and/or Europe and those under clinical developments, the example reported in this article represents only the initial step of an increasing effort aimed at the design of versatile theranostic systems based on porous nanozeolites as functional hosts.

Supporting Information Detailed experimental part, nanocrystals physicochemical characterization, full XPS and TGA results, gel electrophoresis, TEM and confocal microscopy images of both binding and internalization experiments.

Acknowledgements

DB and LDC thanks the EU through the FP7 research-funded SACS project (contract n° 310651). DB acknowledges the FRS-FNRS (FRFC contract n° T.1112.14), the Science Policy Office of the Belgian Federal Government (BELSPO-IAP 7/05 project), the ‘Service Public de Wallonie’ through the “THERAPLUS” project, and the University of Namur (internal funding). RM thanks the FRS-FNRS for his post-doctoral fellowship. EAP and LDC acknowledge financial support from the European Research Council for ERC Advanced Grant (Grant Agreement no. 2009-247365) and from ARC, project Thera-HCC. The authors acknowledge the support of the “Morphology-Imaging” technological platform from the UNamur and thank Noelle Ninane and Catherine Demazy for the technical assistance with the confocal microscope.

Received: ((will be filled in by the editorial staff))

Revised: ((will be filled in by the editorial staff))

Published online: ((will be filled in by the editorial staff))

- [1] a) L. Cheng, C. Wang, L. Feng, K. Yang, Z. Liu, *Chem. Rev.* **2014**, *114*, 10869; b) E. K. Lim, T. Kim, S. Paik, S. Haam, Y. M. Huh, K. Lee, *Chem. Rev.* **2015**, *115*, 327; c) J. Yao, M. Yang, Y. Duan, *Chem. Rev.* **2014**, *114*, 6130; d) V. Biju, *Chem. Soc. Rev.* **2014**, *43*, 744; e) Y. Chen, C. Tan, H. Zhang, L. Wang, *Chem. Soc. Rev.* **2015**, *44*, 2681; f) V. Shanmugam, S. Selvakumar, C. S. Yeh, *Chem. Soc. Rev.* **2014**, *43*, 6254; g) S. Nazir, T. Hussain, A. Ayub, U. Rashid, A. J. MacRobert, *Nanomedicine* **2014**, *10*, 19.
- [2] a) S. E. Jin, H. E. Jin, S. S. Hong, *Biomed. Res. Int.* **2014**, *2014*, 814208; b) G. Y. Tonga, D. F. Moyano, C. S. Kim, V. M. Rotello, *Curr. Opin. Colloid Interface Sci.* **2014**, *19*, 49; c) A. Wicki, D. Witzigmann, V. Balasubramanian, J. Huwyler, *J. Contr. Release* **2015**, *200*, 138; d) R. van der Meel, L. J. C. Vehmeijer, R. J. Kok, G. Storm, E. V. B. van Gaal, *Adv. Drug Deliv. Rev.* **2013**, *65*, 1284; e) R. Lehner, X. Wang, S. Marsch, P. Hunziker, *Nanomedicine* **2013**, *9*, 742; f) E. Lavik, H. Von Recum, *ACS Nano* **2011**, *5*, 3419.
- [3] a) B. T. Luk, L. Zhang, *ACS Appl. Mater. Interfaces* **2014**, *6*, 21859; b) A. Singh, S. K. Sahoo, *Drug Discov. Today* **2014**, *19*, 474; c) T. H. Kim, S. Lee, X. Chen, *Expert Rev. Mol. Diagn.* **2013**, *13*, 257; d) S. Svenson, *Mol. Pharm.* **2013**, *10*, 848.
- [4] a) P. Yang, S. Gai, J. Lin, *Chem. Soc. Rev.* **2012**, *41*, 3679; b) Z. Li, J. C. Barnes, A. Bosoy, J. F. Stoddart, J. I. Zink, *Chem. Soc. Rev.* **2012**, *41*, 2590; c) M. Haase, H. Schäfer, *Angew. Chem. Int. Ed.* **2011**, *50*, 5808.
- [5] a) N. Bertrand, J. Wu, X. Xu, N. Kamaly, O. C. Farokhzad, *Adv. Drug Deliv. Rev.* **2014**, *66*, 2; b) H. Maeda, H. Nakamura, J. Fang, *Adv. Drug Deliv. Rev.* **2013**, *65*, 71.
- [6] a) E. Blanco, H. Shen, M. Ferrari, *Nat. Biotechnol.* **2015**, *33*, 941; b) K. P. García, K. Zarschler, L. Barbaro, J. A. Barreto, W. O'Malley, L. Spiccia, H. Stephan, B. Graham, *Small* **2014**, *10*, 2516.
- [7] a) L. A. Dykman, N. G. Khlebtsov, *Chem. Rev.* **2014**, *114*, 1258; b) H. Kettiger, A. Schipanski, P. Wick, J. Huwyler, *Int. J. Nanomed.* **2013**, *8*, 3255; c) C. Huang, Y. Zhang, H. Yuan, H.

- Gao, S. Zhang, *Nano Lett.* **2013**, *13*, 4546; d) T.-G. Iversen, T. Skotland, K. Sandvig, *Nano Today* **2011**, *6*, 176; e) V. Mailänder, K. Landfester, *Biomacromolecules* **2009**, *10*, 2379; f) H. Hillaireau, P. Couvreur, *Cell Mol. Life Sci.* **2009**, *66*, 2873; g) N. W. S. Kam, Z. Liu, H. Dai, *Angew. Chem. Int. Ed.* **2006**, *45*, 577; h) L. Lacerda, J. Russier, G. Pastorin, M. A. Herrero, E. Venturelli, H. Dumortier, K. T. Al-Jamal, M. Prato, K. Kostarelos, A. Bianco, *Biomaterials* **2012**, *33*, 3334.
- [8] a) B. R. Smith, E. E. B. Ghosn, H. Rallapalli, J. A. Prescher, T. Larson, L. A. Herzenberg, S. S. Gambhir, *Nat. Nanotechnol.* **2014**, *9*, 481; b) M. A. Lameijer, J. Tang, M. Nahrendorf, R. H. J. Beelen, W. J. M. Mulder, *Expert Rev. Mol. Diagn.* **2013**, *13*, 567; c) J. W. Yoo, D. J. Irvine, D. E. Discher, S. Mitragotri, *Nat. Rev. Drug Discov.* **2011**, *10*, 521; d) M. T. Stephan, D. J. Irvine, *Nano Today* **2011**, *6*, 309; e) L. Li, Y. Guan, H. Liu, N. Hao, T. Liu, X. Meng, C. Fu, Y. Li, Q. Qu, Y. Zhang, S. Ji, L. Chen, D. Chen, F. Tang, *ACS Nano* **2011**, *5*, 7462.
- [9] B. Wang, C. V. Galliford, P. S. Low, *Nanomedicine* **2014**, *9*, 313.
- [10] Q. Tu, Y. Zhang, R. Liu, J. C. Wang, L. Li, N. Nie, A. Liu, L. Wang, W. Liu, L. Ren, X. Wang, J. Wang, *Curr. Med. Chem.* **2012**, *19*, 3152.
- [11] a) M. H. El-Dakdouki, D. C. Zhu, K. El-Boubbou, M. Kamat, J. Chen, W. Li, X. Huang, *Biomacromolecules* **2012**, *13*, 1144; b) R. Marega, M. Bergamin, V. Aroulmoji, F. Dinon, M. Prato, E. Murano, *Eur. J. Org. Chem.* **2011**, 5617.
- [12] a) W. Jiang, B. Y. S. Kim, J. T. Rutka, W. C. W. Chan, *Nat. Nanotechnol.* **2008**, *3*, 145; b) L. M. Bareford, P. W. Swaan, *Adv. Drug Deliv. Rev.* **2007**, *59*, 748.
- [13] K. Zarschler, K. Prapainop, E. Mahon, L. Rocks, M. Bramini, P. M. Kelly, H. Stephan, K. A. Dawson, *Nanoscale* **2014**, *6*, 6046.
- [14] a) P. Kirkpatrick, J. Graham, M. Muhsin, *Nat. Rev. Drug Discov.* **2004**, *3*, 549; b) J. Harding, B. Burtness, *Drugs Today* **2005**, *41*, 107.
- [15] a) A. M. Master, A. Sen Gupta, *Nanomedicine* **2012**, *7*, 1895; b) K. Löw, M. Wacker, S. Wagner, K. Langer, H. Von Briesen, *Nanomedicine* **2011**, *7*, 454; c) Y. S. Cho, T. J. Yoon, E.

S. Jang, K. Soo Hong, S. Young Lee, O. Ran Kim, C. Park, Y. J. Kim, G. C. Yi, K. Chang, *Cancer Lett.* **2010**, *299*, 63.

- [16] a) R. Marega, L. Karmani, L. Flamant, P. G. Nageswaran, V. Valembois, B. Masereel, O. Feron, T. V. Borghet, S. Lucas, C. Michiels, B. Gallez, D. Bonifazi, *J. Mater. Chem.* **2012**, *22*, 21305; b) S. Maya, L. G. Kumar, B. Sarmento, N. Sanoj Rejinold, D. Menon, S. V. Nair, R. Jayakumar, *Carbohydr. Polymer.* **2013**, *93*, 661; c) C. R. Patra, R. Bhattacharya, E. Wang, A. Katarya, J. S. Lau, S. Dutta, M. Muders, S. Wang, S. A. Buhrow, S. L. Safgren, M. J. Yaszemski, J. M. Reid, M. M. Ames, P. Mukherjee, D. Mukhopadhyay, *Cancer Res.* **2008**, *68*, 1970; d) C. Liao, Q. Sun, B. Liang, J. Shen, X. Shuai, *Eur. J. Radiol.* **2011**, *80*, 699; e) S. H. Tseng, M. Y. Chou, I. M. Chu, *Int. J. Nanomed.* **2015**, *10*, 3663; f) S. Maya, B. Sarmento, V. K. Lakshmanan, D. Menon, R. Jayakumar, *J. Biomed. Nanotechnol.* **2014**, *10*, 1416; g) V. G. Deepagan, B. Sarmento, D. Menon, A. Nascimento, A. Jayasree, M. Sreeranganathan, M. Koyakutty, S. V. Nair, J. Rangasamy, *Nanomedicine* **2012**, *7*, 507; h) H. W. Kao, Y. Y. Lin, C. C. Chen, K. H. Chi, D. C. Tien, C. C. Hsia, W. J. Lin, F. D. Chen, M. H. Lin, H. E. Wang, *Nanotechnology* **2014**, *25*; i) M. Kaluzova, A. Bouras, R. Machaidze, C. G. Hadjipanayis, *Oncotarget* **2015**, *6*, 8788; j) S. Bhattacharyya, R. D. Singh, R. Pagano, J. D. Robertson, R. Bhattacharya, P. Mukherjee, *Angew. Chem. Int. Ed.* **2012**, *51*, 1563; k) S. Bhattacharyya, R. Bhattacharya, S. Curley, M. A. McNiven, P. Mukherjee, *Proc. Nat. Acad. Sci USA* **2010**, *107*, 14541.
- [17] a) L. Karmani, D. Labar, V. Valembois, V. Bouchat, P. G. Nageswaran, A. Bol, J. Gillart, P. Leveque, C. Bouzin, D. Bonifazi, C. Michiels, O. Feron, V. Gregoire, S. Lucas, T. Vander Borghet, B. Gallez, *Contrast Media Mol. Imaging* **2013**, *8*, 402; b) J. A. Khan, R. A. Kudgus, A. Szabolcs, S. Dutta, E. Wang, S. Cao, G. L. Curran, V. Shah, S. Curley, D. Mukhopadhyay, J. D. Robertson, R. Bhattacharya, P. Mukherjee, *PLoS ONE* **2011**, *6*, e20347; c) C. G. Hadjipanayis, R. Machaidze, M. Kaluzova, L. Wang, A. J. Schuette, H. Chen, X. Wu, H. Mao,

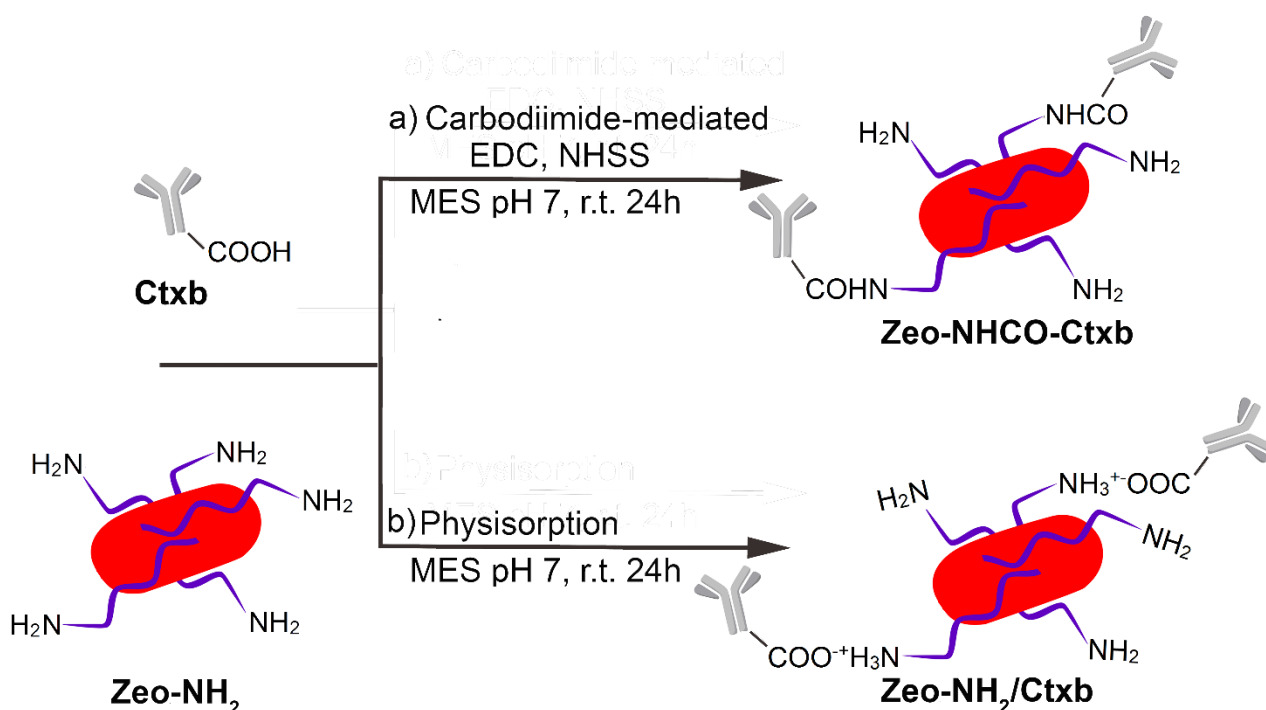
- Cancer Res.* **2010**, *70*, 6303; d) T. Reuveni, M. Motiei, Z. Romman, A. Popovtzer, R. Popovtzer, *Int. J. Nanomed.* **2011**, *6*, 2859.
- [18] H. Jaganathan, B. Godin, *Adv. Drug Deliv. Rev.* **2012**, *64*, 1800.
- [19] a) F. Chen, H. Hong, Y. Zhang, H. F. Valdovinos, S. Shi, G. S. Kwon, C. P. Theuer, T. E. Barnhart, W. Cai, *ACS Nano* **2013**, *7*, 9027; b) C. P. Tsai, C. Y. Chen, Y. Hung, F. H. Chang, C. Y. Mou, *J. Mater. Chem.* **2009**, *19*, 5737; c) E. Secret, K. Smith, V. Dubljevic, E. Moore, P. Macardle, B. Delalat, M. L. Rogers, T. G. Johns, J. O. Durand, F. Cunin, N. H. Voelcker, *Adv. Healthcare Mater.* **2013**, *2*, 718.
- [20] a) M. M. Tsotsalas, K. Kopka, G. Luppi, S. Wagner, M. P. Law, M. Schäfers, L. De Cola, *ACS Nano* **2010**, *4*, 342; b) C. A. Strassert, M. Otter, R. Q. Albuquerque, A. Hone, Y. Vida, B. Maier, L. De Cola, *Angew. Chem. Int. Ed.* **2009**, *48*, 7928; c) M. Tsotsalas, M. Busby, E. Gianolio, S. Aime, L. De Cola, *Chem. Mater.* **2008**, *20*, 5888; d) M. Busby, H. Kerschbaumer, G. Calzaferri, L. De Cola, *Adv. Mater.* **2008**, *20*, 1614; e) Z. Popović, M. Otter, G. Calzaferri, L. De Cola, *Angew. Chem. Int. Ed.* **2007**, *46*, 6188; f) A. Bertucci, H. Lülff, D. Septiadi, A. Manicardi, R. Corradini, L. De Cola, *Adv. Healthcare Mater.* **2014**, *3*, 1812; g) N. S. Kehr, K. Riehemann, J. El-Gindi, A. Schäfer, H. Fuchs, H. J. Galla, L. De Cola, *Adv. Funct. Mater.* **2010**, *20*, 2248; h) J. El-Gindi, K. Benson, L. De Cola, H. J. Galla, N. Seda Kehr, *Angew. Chem. Int. Ed.* **2012**, *51*, 3716.
- [21] Z. Li, J. Hüve, C. Krampe, G. Luppi, M. Tsotsalas, J. Klingauf, L. De Cola, K. Riehemann, *Small* **2013**, *9*, 1809.
- [22] O. Bossart, L. De Cola, S. Welter, G. Calzaferri, *Chemistry* **2004**, *10*, 5771.
- [23] a) R. Marega, F. De Leo, F. Pineux, J. Sgrignani, A. Magistrato, A. D. Naik, Y. Garcia, L. Flamant, C. Michiels, D. Bonifazi, *Adv. Funct. Mater.* **2013**, *23*, 3173; b) F. Pineux, R. Marega, A. Stopin, A. La Torre, Y. Garcia, E. Devlin, C. Michiels, A. N. Khlobystov, D. Bonifazi, *Nanoscale* **2015**, *7*, 20474.

- [24] a) A. A. Shemetov, I. Nabiev, A. Sukhanova, *ACS Nano* **2012**, *6*, 4585; b) C. D. Walkey, W. C. W. Chan, *Chem. Soc. Rev.* **2012**, *41*, 2780; c) L. Treuel, G. U. Nienhaus, *Biophys. Rev.* **2012**, *4*, 137; d) P. D. Pino, B. Pelaz, Q. Zhang, P. Maffre, G. U. Nienhaus, W. J. Parak, *Mater. Horizons* **2014**, *1*, 301; e) M. Mahmoudi, I. Lynch, M. R. Ejtehadi, M. P. Monopoli, F. B. Bombelli, S. Laurent, *Chem. Rev.* **2011**, *111*, 5610; f) M. P. Monopoli, D. Walczyk, A. Campbell, G. Elia, I. Lynch, F. Baldelli Bombelli, K. A. Dawson, *J. Am. Chem. Soc.* **2011**, *133*, 2525; g) I. Lynch, K. A. Dawson, *Nano Today* **2008**, *3*, 40; h) M. P. Monopoli, C. Åberg, A. Salvati, K. A. Dawson, *Nat. Nanotechnol.* **2012**, *7*, 779; i) T. Cedervall, I. Lynch, S. Lindman, T. Berggård, E. Thulin, H. Nilsson, K. A. Dawson, S. Linse, *Proc. Nat. Acad. Sci USA* **2007**, *104*, 2050; j) M. Lundqvist, J. Stigler, G. Elia, I. Lynch, T. Cedervall, K. A. Dawson, *Proc. Nat. Acad. Sci USA* **2008**, *105*, 14265.
- [25] R. Marega, V. Aroulmoji, M. Bergamin, L. Feruglio, F. Dinon, A. Bianco, E. Murano, M. Prato, *ACS Nano* **2010**, *4*, 2051.
- [26] a) F. De Leo, A. Magistrato, D. Bonifazi, *Chem. Soc. Rev.* **2015**, *44*, 6916; b) F. De Leo, J. Sgrignani, D. Bonifazi, A. Magistrato, *Chem. Eur. J.* **2013**, *19*, 12281.
- [27] a) J. Nam, N. Won, J. Bang, H. Jin, J. Park, S. Jung, S. Jung, Y. Park, S. Kim, *Adv. Drug Deliv. Rev.* **2013**, *65*, 622; b) C. M. Beddoes, C. P. Case, W. H. Briscoe, *Adv. Colloid Interface Sci.* **2015**, *218*, 48; c) L. C. Cheng, X. Jiang, J. Wang, C. Chen, R. S. Liu, *Nanoscale* **2013**, *5*, 3547; d) X. Duan, Y. Li, *Small* **2013**, *9*, 1521.
- [28] G. Maiorano, S. Sabella, B. Sorce, V. Brunetti, M. A. Malvindi, R. Cingolani, P. P. Pompa, *ACS Nano* **2010**, *4*, 7481.
- [29] a) B. Pelaz, P. Del Pino, P. Maffre, R. Hartmann, M. Gallego, S. Rivera-Fernández, J. M. De La Fuente, G. U. Nienhaus, W. J. Parak, *ACS Nano* **2015**, *9*, 6996; b) Q. Dai, C. Walkey, W. C. W. Chan, *Angew. Chem. Int. Ed.* **2014**, *53*, 5093; c) V. Torrisi, A. Graillet, L. Vitorazi, Q. Crouzet, G. Marletta, C. Loubat, J. F. Berret, *Biomacromolecules* **2014**, *15*, 3171; d) D. Pozzi,

- V. Colapicchioni, G. Caracciolo, S. Piovesana, A. L. Capriotti, S. Palchetti, S. De Grossi, A. Riccioli, H. Amenitsch, A. Laganà, *Nanoscale* **2014**, *6*, 2782.
- [30] K. J. Ong, T. J. MacCormack, R. J. Clark, J. D. Ede, V. A. Ortega, L. C. Felix, M. K. M. Dang, G. Ma, H. Fenniri, J. G. C. Veinot, G. G. Goss, *PLoS ONE* **2014**, *9*, e90650.
- [31] a) T. Lühmann, M. Rimann, A. G. Bittermann, H. Hall, *Bioconj. Chem.* **2008**, *19*, 1907; b) M. R. Lorenz, V. Holzapfel, A. Musyanovych, K. Nothelfer, P. Walther, H. Frank, K. Landfester, H. Schrezenmeier, V. Mailänder, *Biomaterials* **2006**, *27*, 2820; c) M. Yu, S. Jambhrunkar, P. Thorn, J. Chen, W. Gu, C. Yu, *Nanoscale* **2013**, *5*, 178; d) A. Fercher, S. M. Borisov, A. V. Zhdanov, I. Klimant, D. B. Papkovsky, *ACS Nano* **2011**, *5*, 5499; e) C. Yu, Y. Hu, J. Duan, W. Yuan, C. Wang, H. Xu, X. D. Yang, *PLoS ONE* **2011**, *6*, e24077; f) Y. Ibuki, T. Toyooka, in *Nanotoxicity: Methods and Protocols* (Ed.: J. Reineke), Humana Press, Totowa, NJ, **2012**, Ch. 11; g) C. Gottstein, G. Wu, B. J. Wong, J. A. Zasadzinski, *ACS Nano* **2013**, *7*, 4933.
- [32] a) S. E. A. Gratton, P. A. Ropp, P. D. Pohlhaus, J. C. Luft, V. J. Madden, M. E. Napier, J. M. DeSimone, *Proc. Nat. Acad. Sci USA* **2008**, *105*, 11613; b) R. Agarwal, V. Singh, P. Journey, L. Shi, S. V. Sreenivasan, K. Roy, *Proc. Nat. Acad. Sci USA* **2013**, *110*, 17247; c) A. M. Bannunah, D. Vllasaliu, J. Lord, S. Stolnik, *Mol. Pharm.* **2014**, *11*, 4363.
- [33] E. Macia, M. Ehrlich, R. Massol, E. Boucrot, C. Brunner, T. Kirchhausen, *Develop. Cell* **2006**, *10*, 839.
- [34] L. H. Wang, K. G. Rothberg, R. G. W. Anderson, *J. Cell Biol.* **1993**, *123*, 1107.
- [35] D. Vercauteren, R. E. Vandenbroucke, A. T. Jones, J. Rejman, J. Demeester, S. C. De Smedt, N. N. Sanders, K. Braeckmans, *Mol. Ther.* **2010**, *18*, 561.
- [36] M. Koivusalo, C. Welch, H. Hayashi, C. C. Scott, M. Kim, T. Alexander, N. Touret, K. M. Hahn, S. Grinstein, *J. Cell Biol.* **2010**, *188*, 547.
- [37] M. A. Jordan, *Curr. Med. Chem.* **2002**, *2*, 1.

- [38] L. Henriksen, M. V. Grandal, S. L. Knudsen, B. van Deurs, L. M. Grovdal, *PLoS ONE* **2013**, *8*, e58148.
- [39] M. Srinivasarao, C. V. Galliford, P. S. Low, *Nat. Rev. Drug Discov.* **2015**, *14*, 203.

FIGURES



Scheme 1. Synthetic strategies for immobilizing Ctxb onto zeolite nanocrystals through carbodiimide-mediated (a) or physisorption-based (b) routes. EDC is N-(3-Dimethylaminopropyl)-N'-ethylcarbodiimide hydrochloride, NHSS is N-hydroxysulfosuccinimide, and MES is 2-(N-morpholino)ethanesulfonic acid buffer.

Table 1. Summarization of the physicochemical properties of the zeolite nanomaterials.

Entry	Sample	DLS (peak, PDI ^a)	ζ potential [mV] ^{a,b}
1	Zeo	56 nm, 0.319 ^b	-24.24
2	Zeo-NH ₂	86 nm, 0.252 ^b ; 110 nm, 0.113 ^c	-22.65
3	Zeo-NHCO-Ctxb	117 nm, 0.300 ^c	-35.73
4	Ctxb	17 nm, 0.178 ^b	-8.89

^a): PDI = polydispersity index; ^b): values obtained from water dispersions; ^c): values obtained from dispersions in serum supplemented biological medium.

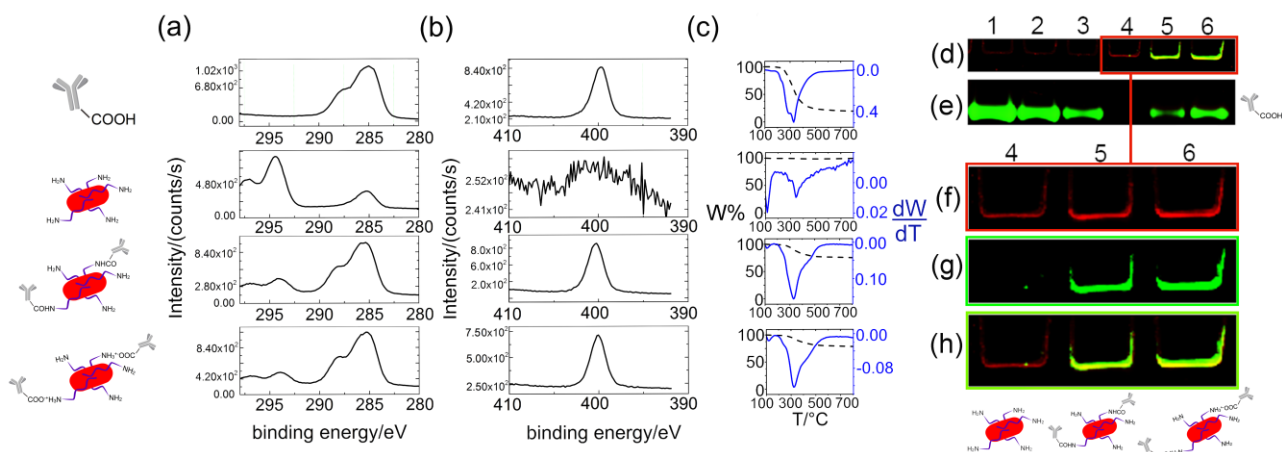


Figure 1. XPS high-resolution spectra for the C1s (a) and N1s (b) regions and TGA profiles under N₂ flow at 90 mL min⁻¹ (c) for Ctxb alone, Zeo-NH₂, Zeo-NHCO-Ctxb and Zeo-NH₂/Ctxb. Two-channel ($\lambda_{1\text{exc}} = 488$ nm and $\lambda_{1\text{em}} = 500$ nm; $\lambda_{2\text{exc}} = 633$ nm and $\lambda_{2\text{em}} = 670$ nm) fluorescence images of the gel lanes (1-6) after electrophoresis (d-h). Ctxb was loaded on lanes 1, 2 and 3, while Zeo-NH₂, Zeo-NHCO-Ctxb and Zeo-NH₂/Ctxb respectively on lanes 4, 5 and 6. Overlaid fluorescence signals located in the deposition area (d) and Ctxb moiety migration band (e). Individual fluorescence at the deposition area (lanes 4,5,6) as revealed in the red channel (f), green channel (g), and overlaid channel intensities (h). Full gel revelation is reported in S4.

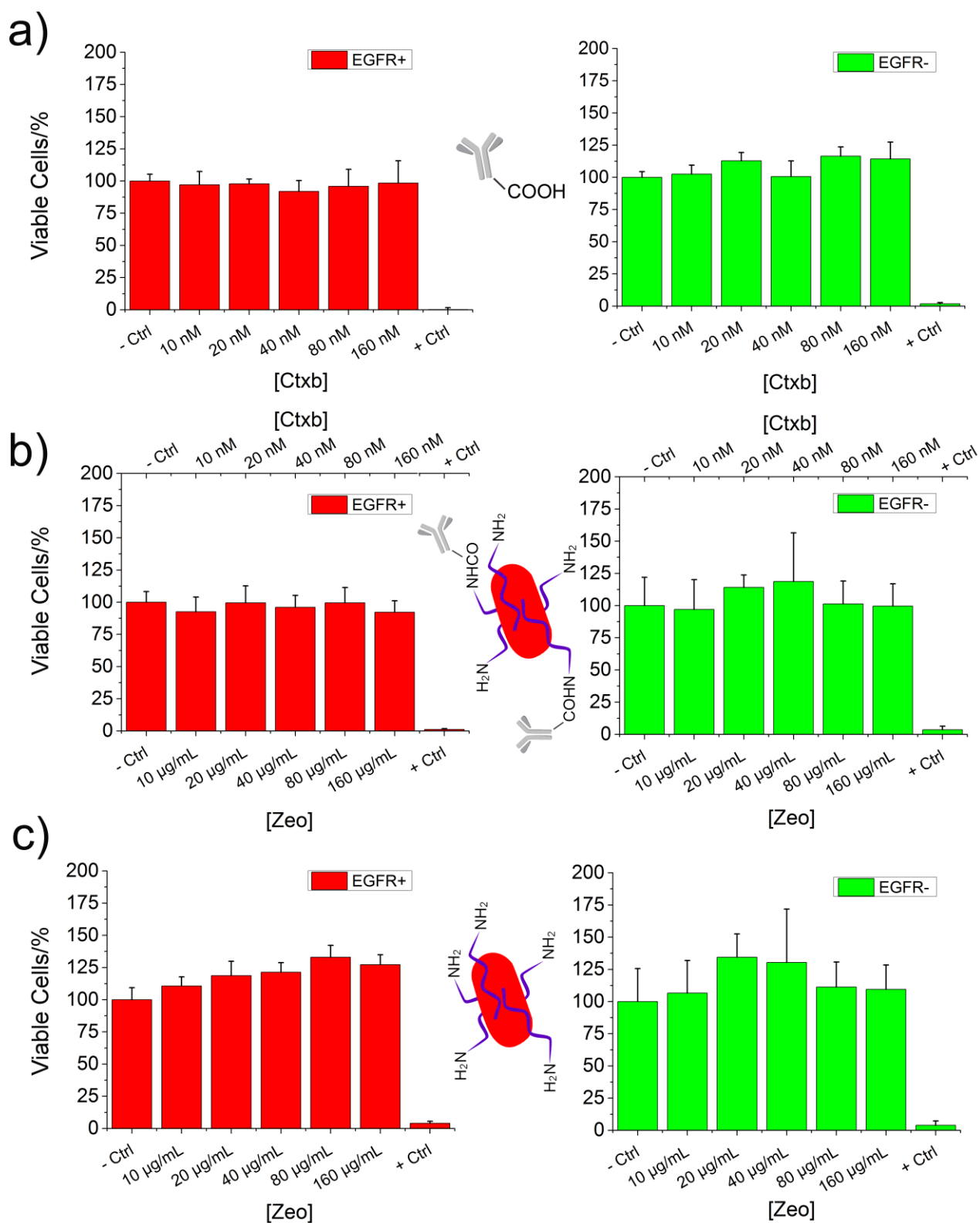


Figure 2. Cell viability assessment by MTS assay after 24h incubation with Ctxb (a), Zeo-NHCO-Ctxb (b), and Zeo-NH₂ (c). Results are expressed as mean \pm s.d. (n=4).

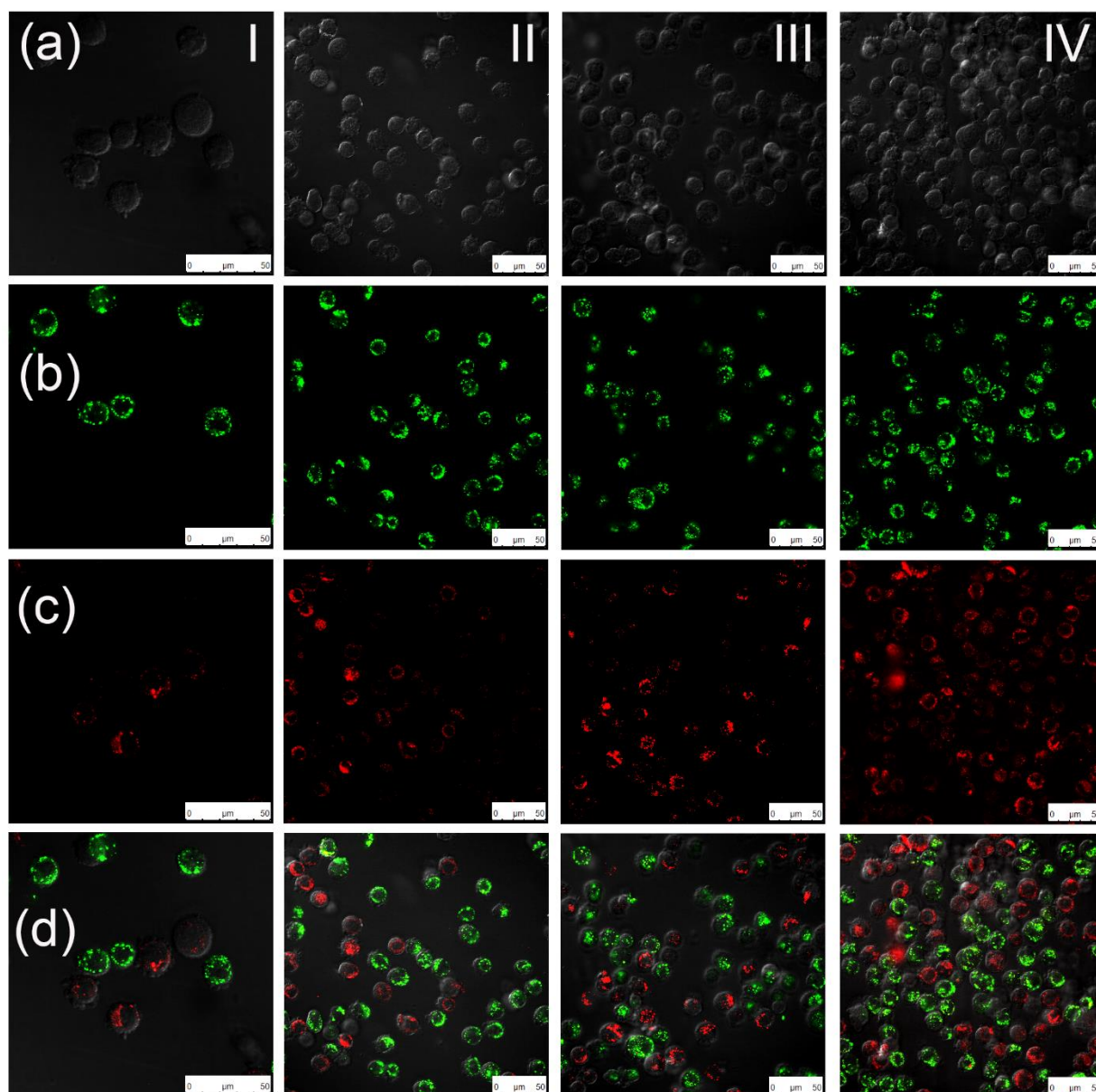


Figure 3. Confocal microscopy images of different fields (I-IV) of a suspension of EGFR⁺ cells and green fluorescently labelled EGFR⁻ cells after incubation (3 minutes) with Zeo-NHCO-Ctxb 0.4 mgmL⁻¹. Individual channel intensity (DIC (a), at $\lambda_{\text{exc}} = 488 \text{ nm}$ (b), and $\lambda_{\text{exc}} = 633 \text{ nm}$ (c)) along with the overlaid images (d). Image scale bars are 50 μm .

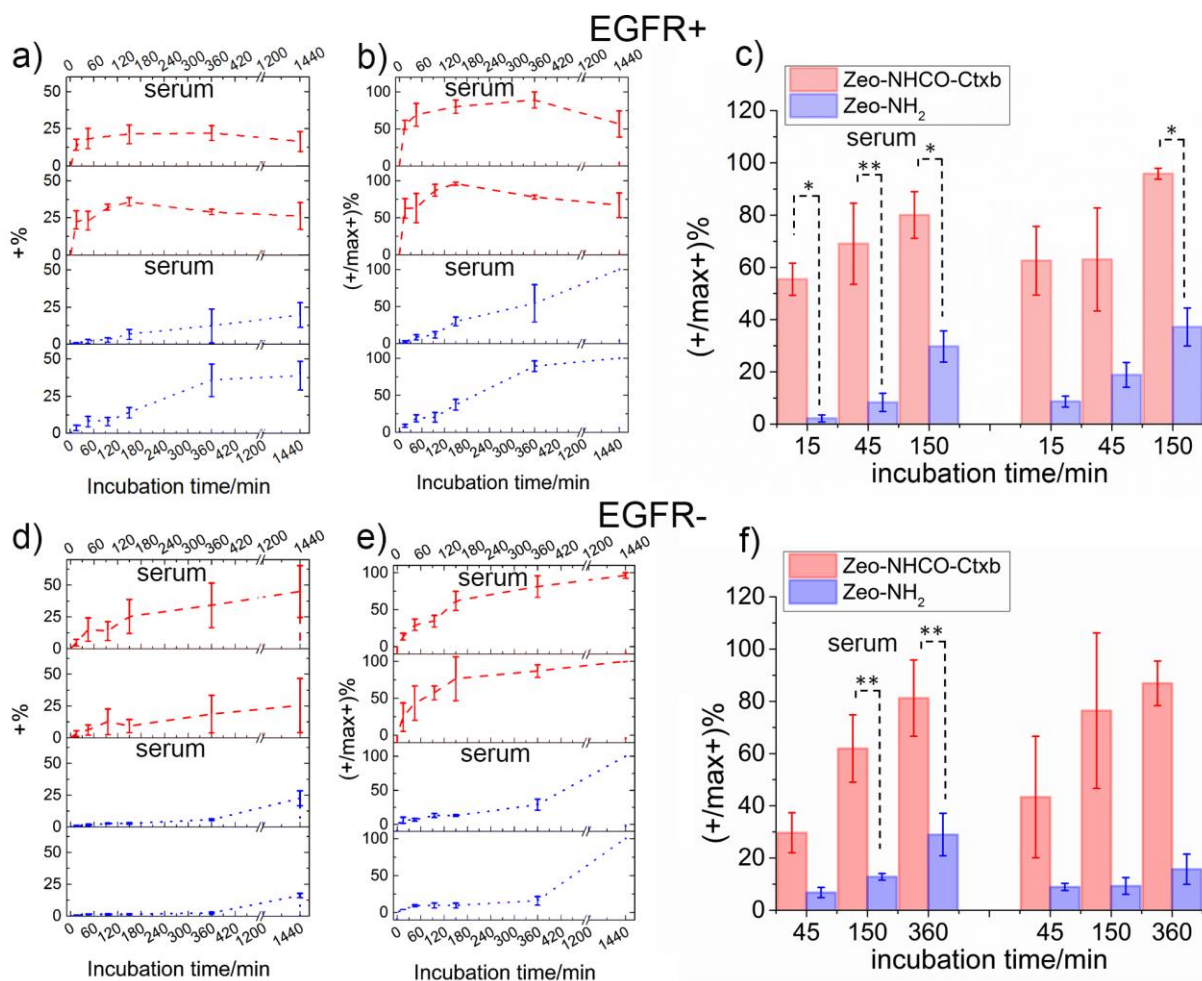


Figure 4. Results of the time-dependent nanocrystal uptake evaluation by flow cytometry. Absolute proportion of fluorescently stained cells over total cell population (+%, a, d) and normalized values ((+/max+)%, b, e), along with one-way ANOVA of the resulting dataset (c, f) on the EGFR+ cell (a, b, c) or EGFR- cell (d, e, f) population. The red-dashed traces result from experiments performed with Zeo-NHCO-Ctxb, while the blue-dotted ones are linked to the use of Zeo-NH₂. In both instances, the results originating from the incubation in the presence of 10% serum are labelled in each graph. * = $p < 0.05$, ** = $p < 0.01$. Data are reported as mean \pm s.e.m. (n=3 independent sets of experiments).

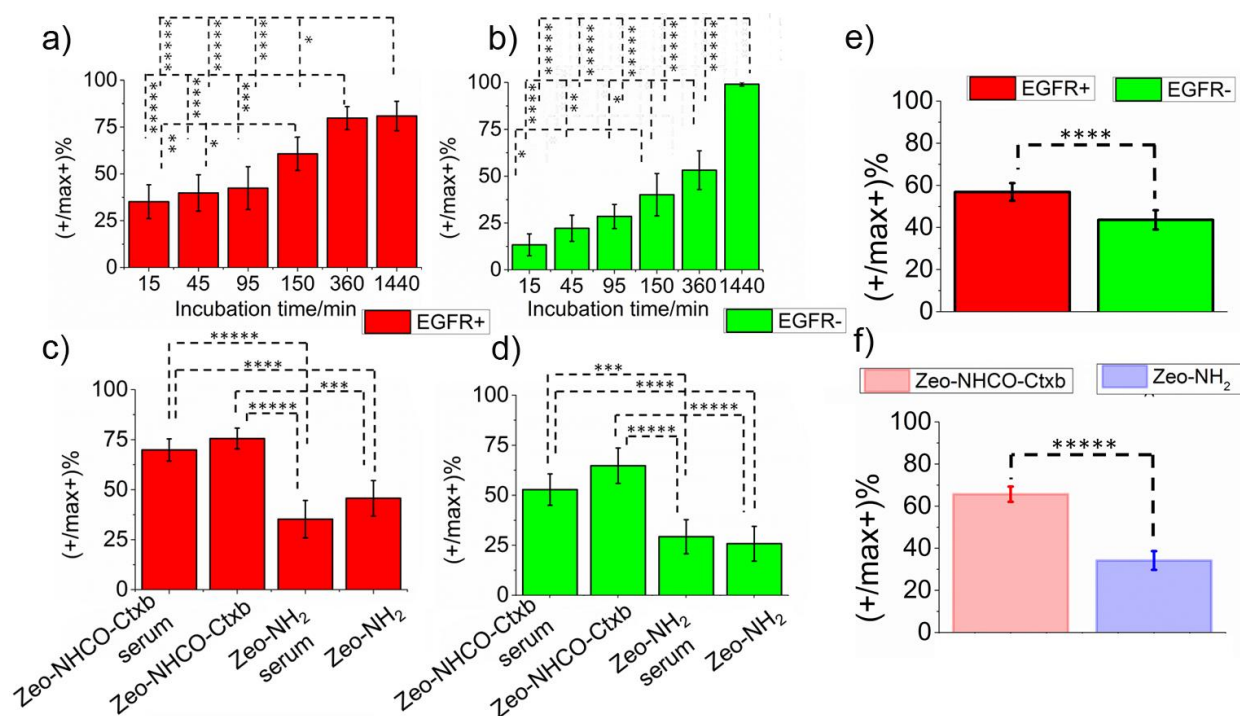


Figure 5. Results of the time-dependent zeolite nanocrystal uptake, as assessed by flow cytometry. 2-way ANOVA after grouping by the factors “incubation time” (a, b) or “nanocrystal biological interface” (c, d) on the individual dataset of EGFR+ cells (a, c) or EGFR- cells (b, d). 2-way ANOVA of the whole EGFR+ and EGFR- cells dataset after grouping by the factors “cell type” (e), or “nanomaterial” (f) against all the other respective incubation parameters. * = $p < 0.05$, ** = $p < 0.01$, *** = $p < 0.001$, **** = $p < 0.0001$, ***** = $p < 0.00001$. Data are reported as mean \pm s.e.m. ($n=3$ independent sets of experiments).

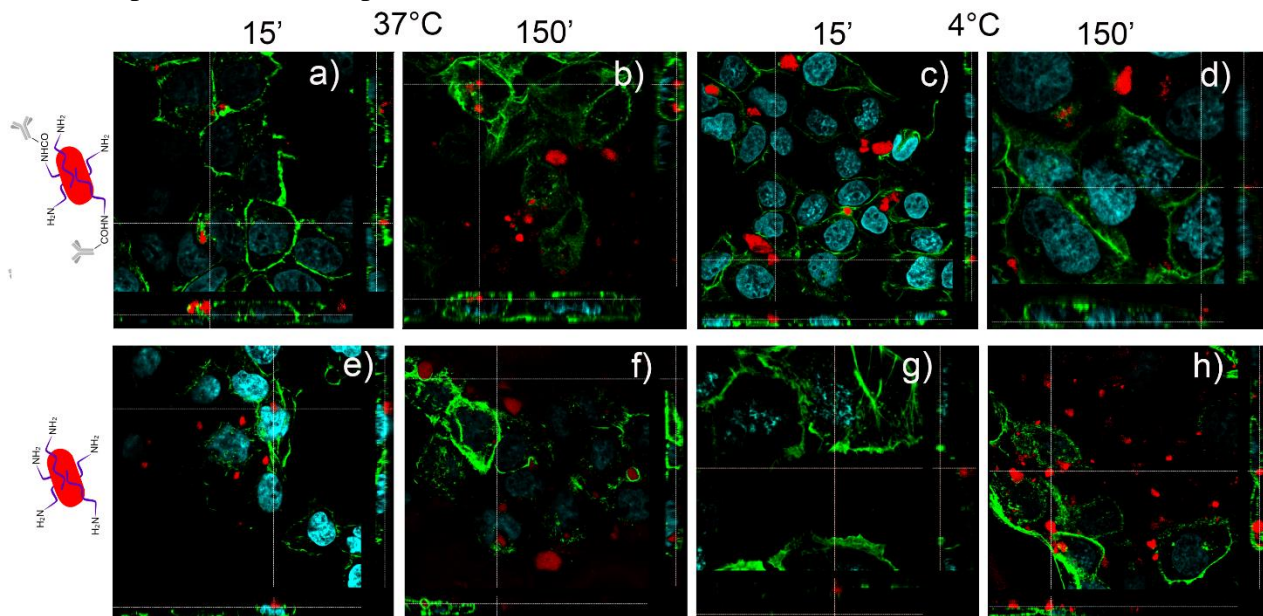


Figure 6. Optical sectioning reporting the fluorescence intensities from nuclei (λ_{exc} 400 nm, cyan), actin filaments (λ_{exc} 488 nm, green) and zeolite nanocrystals (λ_{exc} 561 nm, red). Representative images of adherent EGFR+ cells after addition of Zeo-NHCO-Ctxb (a, b, c, d) or Zeo-NH₂ (e, f, g, h) at 37 °C (a, b, e, f) or 4 °C (c, d, g, h), 15 minutes (a, c, e, g) or 150 minutes (b, d, f, h) after incubation. The composed images show three parts: the bottom image is the X-Z projection, the right image is the Y-Z projection and the main image is the X-Y projection, all relative to the white lines identifying the XYZ positioning along the 3D z-stack.

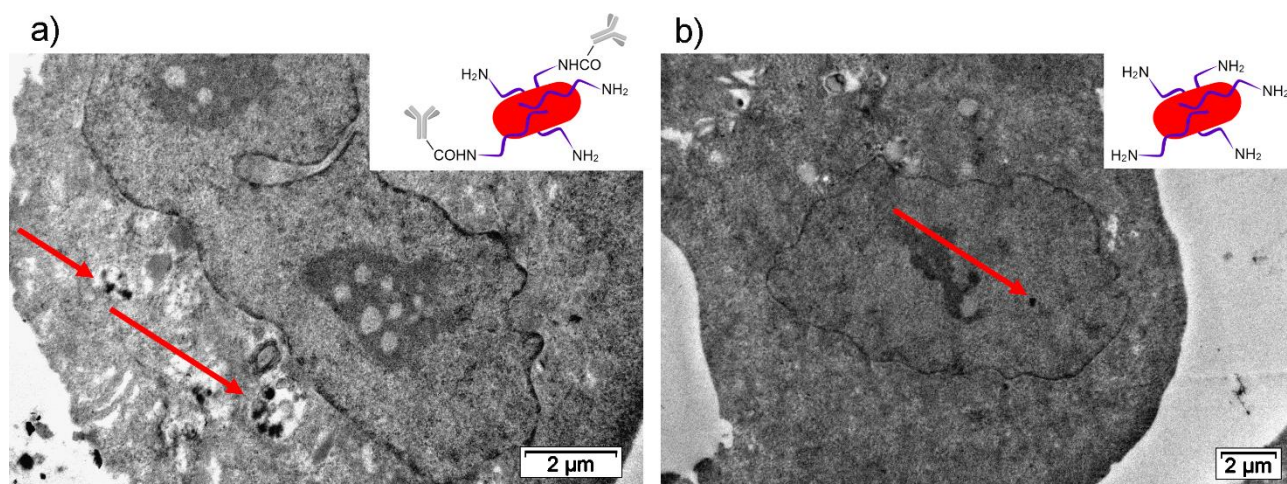


Figure 7. TEM images of EGFR+ cells incubated for 150 minutes with Zeo-NHCO-Ctxb (a) or Zeo-NH₂ (b). Red arrows point toward some of the clusters that, according to their morphology and imaging contrast, are compatible with zeolite nanocrystals (See Figure S13 for additional images).

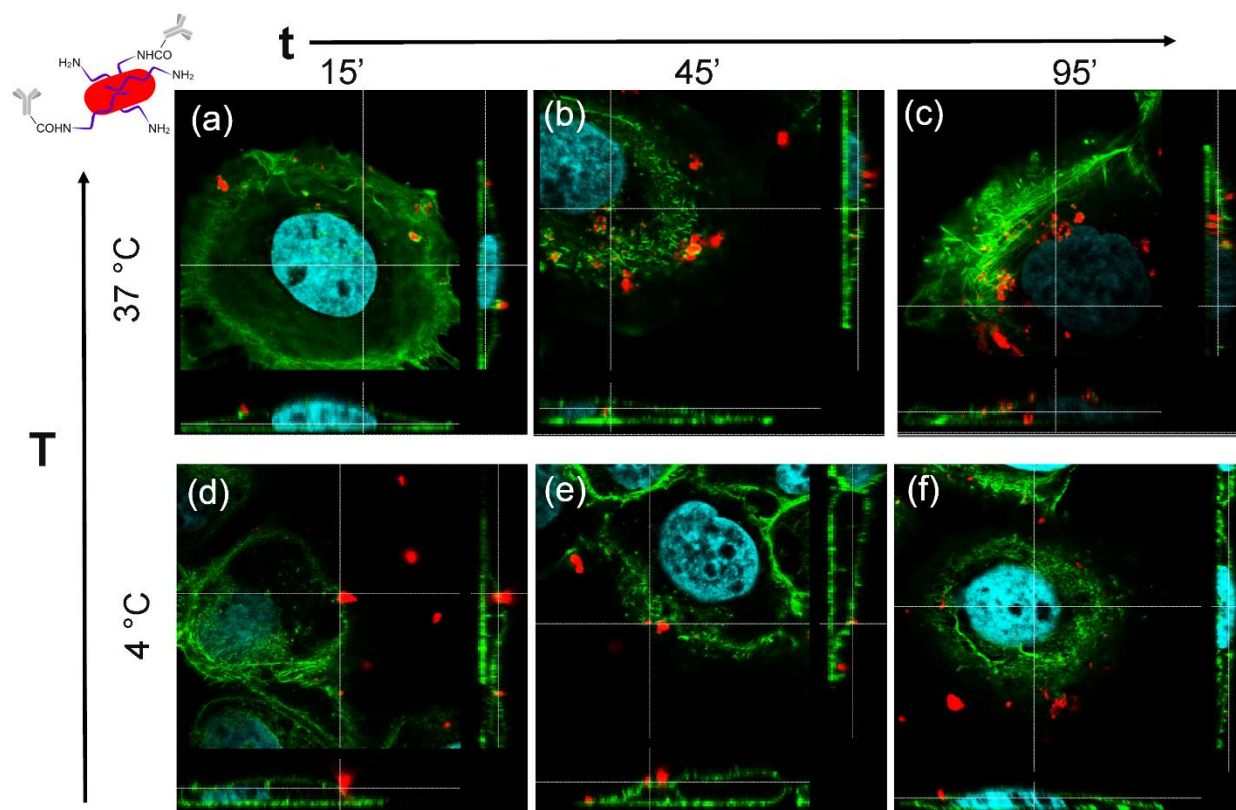


Figure 8. Optical sectioning reporting the fluorescence intensities from nuclei ($\lambda_{\text{exc}} = 400$ nm, cyan), actin filaments ($\lambda_{\text{exc}} = 488$ nm, green) and zeolite nanocrystals ($\lambda_{\text{exc}} = 561$ nm, red color). Representative images of adherent EGFR+ cells upon addition of Zeo-NHCO-Ctxb at 37 °C and after different incubation times (a = 15 minutes, b = 45 minutes, and c = 95 minutes), or after incubation at 4 °C (d = 15 minutes, e = 45 minutes, and f = 95 minutes). The composed images show three parts: the bottom image is the X-Z projection, the right image is the Y-Z projection and the main image is the X-Y projection, all relative to the white lines identifying the XYZ positioning along the 3D z-stack.

Bioconjugates do it better! Zeolite nanocrystals functionalized with tumor-targeting Cetuximab antibody undergo very fast cellular uptake by cancer cells, paving the way for the design of functional nanomaterials as potential theranostic platforms.

Nanomaterial uptake

R. Marega, E. A. Prasetyanto, C. Michiels, L. De Cola* and D. Bonifazi*

Fast targeting and cancer cell uptake of luminescent antibody-nanozeolite bioconjugates

